



ELSEVIER

Contents lists available at [SciVerse ScienceDirect](http://www.sciencedirect.com)

Wear

journal homepage: www.elsevier.com/locate/wear

Thermo-chemical wear model and worn tool shapes for single-crystal diamond tools cutting steel

B.M. Lane^{a,*}, T.A. Dow^b, R. Scattergood^b

^a National Institute of Standards and Technology, 100 Bureau Drive, MS 8220, Gaithersburg, MD 20899, USA

^b North Carolina State University, Raleigh, NC 27695, USA

ARTICLE INFO

Article history:

Received 25 July 2012

Received in revised form

22 January 2013

Accepted 26 February 2013

Available online 6 March 2013

Keywords:

Diamond tool

Electron microscopy

Diffusion

FEM

ABSTRACT

An Arrhenius-type thermochemical wear model proposed by past researchers is evaluated for predicting diamond tool wear when machining low carbon steel. Tool temperature values are determined using finite element modeling. These temperatures are related to tool wear measured after diamond turning tests on a low carbon steel workpiece to determine constants in the Arrhenius-type model. Measured tool wear shows a transition in worn tool shape from low speed (1 mm/s) to high speed (4 m/s) machining tests. Model results show a minimum value of wear per cutting distance occurs at a cutting speed of 2.5 m/s. The model also gives an activation energy between 25.0 kJ/mol and 29.3 kJ/mol. In addition, this model is used to explain experimental results obtained by others researching chemical wear of diamond.

© 2013 Elsevier B.V. All rights reserved.

1. Introduction

Diamond turning (DT) is a manufacturing process that utilizes a single crystal diamond tool to form geometrically precise components used in medical, defense, research, and other industries. These components typically have a surface finish less than 10 nm and/or a form error less than 0.5 μm . Consensus was made early in diamond turning history that ferrous materials could not be diamond turned with conventional methods due to the chemical interaction between diamond and iron [1,2]. Multiple unconventional methods have been incorporated to allow diamond turning of steels with varied levels of success including cryogenic turning, turning in carbon-saturated environments, or ultrasonic vibration-assisted machining [3–5]. These methods were invented to address identified contributors to thermo-chemical diamond wear. Though there is a basic understanding of why these special methods work, they cannot be optimized without a more thorough understanding of the chemical reaction mechanism and process parameters that have greatest effect on tool wear. Despite over four decades of research investigating diamond wear when rubbing or machining ferrous alloys, few have attempted to model the thermo-chemical reaction and directly relate this model to actual measurements of a diamond used to machine a steel sample.

There are two main reasons why thermo-chemical tool wear of ultraprecision machine tools is difficult to model empirically. The first reason is the difficulty of measurement of wear. The wear is typically sub-micron in scale. To measure wear at this scale requires use of special tools such as a scanning electron microscope (SEM) or an atomic force microscope (AFM). Both have advantages and disadvantages. For example, diamond is a poor conductor and is subject to charging in an SEM. In addition, SEM provides two-dimensional (2D) images, which can only resolve three-dimensional (3D) wear or worn volume with special techniques or analysis. Asai et al. used a scanning electron microscope with two secondary electron detectors to obtain the 3D orientation of a line scanned over the diamond tool edge [6]. This required special equipment, however, that is uncommon in most machines. Several authors have used an AFM to measure the cutting edge of a diamond tool [7,8]. In an AFM, the probe tip can become damaged or worn, and periodic measurement of a reference artifact may be necessary. Gao et al. noted the difficulty in aligning a diamond edge with the AFM probe tip, so they developed a procedure to align both the diamond and probe tip at the focal point of a diode laser [9]. In addition to SEM and AFM, indirect methods such as indenting worn tools into softer material and measuring the indentation have been used [10]. This paper utilizes a technique called electron beam-induced deposition (EBID), which is performed in an SEM [11–13]. Normally, the planar view of an SEM image cannot resolve cross-sectional wear geometry of a diamond tool edge and can only provide qualitative comparison. The EBID method uses hydrocarbon contamination growth laid perpendicular to the

* Corresponding author. Tel.: +1 301 975 5471; fax: +1 301 975 8058.
E-mail address: brandon.lane@nist.gov (B.M. Lane).

diamond edge as a contrasting agent that allows the 2D cross-section to be discerned in the SEM image. This geometry replicates wear geometry as if being viewed directly down the cutting edge. The SEM image, with tool cross-section, is digitized and analyzed in Matlab¹ to calculate 2D worn cross-sectional area. Worn tool cross-sections from multiple tool measurements can also be aligned with one another to directly compare wear results. Most diamond tool wear, however, is difficult to characterize since the edge recession is on the same order as the depth of cut (sub-micrometer to tens of micrometers), while the contact length may be several orders of magnitude longer. By utilizing a unique cutting geometry in this study, the resulting wear is kept constant along the cutting edge. Thus, wear volume is simply the cross-sectional wear area multiplied by the width of the wear.

The second reason thermo-chemical diamond tool wear is difficult to model is the lack of knowledge of process-induced temperatures, specifically at the diamond and chip contact. Diamond tool temperature measurement is difficult for many of the same reasons as macro-scale cutting temperatures. DT cutting speeds are on the order of 1 m/s or above, while typical cutting depths and feeds are below 50 μm and 5 $\mu\text{m}/\text{rev}$, respectively. High speed infrared (IR) videography is used to observe temperatures in non-ultraprecision turning, but the scale of DT depth of cut and chip thickness is at or below infrared wavelengths (0.75 μm to 10 μm or more). This poses spatial resolution limitations due to IR light diffraction [14]. Rather than relying on IR methods, Yoshioka et al. used a resistance-type platinum film micro-thermometer mounted on the rake face of the tool [15]. Temperature measured at the sensor location would be dramatically less than in the chip-tool contact zone where thermo-chemical wear would occur due to the high conductivity of diamond and resulting steep temperature gradient. Ueda et al. claimed to have measured diamond tool temperature at the chip-tool contact [16]. They used a two-color optical pyrometer to measure infrared radiation that passed through the diamond from the cutting zone. This single-point measurement technique still required a finite element method (FEM) temperature model to relate single point pyrometer measurement to a predicted temperature distribution on the tool rake face. Komanduri et al. later used Ueda's cutting parameters in an extensive analytical heat transfer model and obtained agreeable temperature values [17–19]. These measurements and calculations determined peak diamond temperatures below 210 °C at up to 10.3 m/s cutting speed on Al and Cu workpieces. This is well below non-ultraprecision turning temperatures with carbide or ceramic tools which typically experience temperatures above 1000 °C [20]. This paper utilizes FEM using the commercial code AdvantEdge by Third Wave Systems to obtain tool temperatures. FEM studies of diamond turning have existed since the late 1980s, but most of these studies focus more on predicting surface residual stress than on tool temperature or wear [21–23]. These models may neglect temperature and strain-rate dependent change to material flow stress in the chip [24], frictional heating between the chip and tool [16], or completely neglect heat transfer into the tool altogether [25,26]. Using the commercial FEM code, we accounted for each of these factors.

Tool wear measurements and predicted temperatures may be used to build a chemical wear model which predicts diamond tool wear on low-carbon steel. This paper presents such a model based on the Arrhenius equation, also referred to as the diffusive law.

This model is similar to models previously proposed by others. However, these models historically have not been used for diamond turning due to the inherent difficulties measuring wear and predicting tool temperatures. Empirical results for this model are obtained using a novel orthogonal machining setup that utilizes straight-edged diamond tools and narrow workpiece material that is thinner than the cutting edge. Tool temperatures are obtained through finite element models that mimic the cutting experiments using the commercial FEM code. Tool wear is measured via the EBID method. Wear measurements are coupled with predicted tool temperature to determine the activation energy for the chemical wearing process. Results from these experiments correlate to other researcher's observations, indicating that the Arrhenius type behavior they predicted does indeed describe diamond tool wear on ferrous workpiece materials.

2. Arrhenius-type tool wear models

Ikawa and Tanaka were the first to propose that diamond grit wear when grinding iron was mainly affected by a thermally activated graphitization and diffusion into the ferrous workpiece material [1]. This was followed by Komanduri and Shaw, who observed diffused carbon at the bottom of grooves made in pure iron after scored by synthetic diamond grit [27]. Previous research of macro-scale (carbide, ceramic, high speed steel, etc.) tool wear had already developed temperature-dependant wear models that resembled the Arrhenius law of diffusion [28,29], but Ikawa's and Komanduri's grinding studies did not mention any governance by a diffusive law. Early researchers of diamond tool wear on ferrous alloys mentioned diffusion or chemical reaction, but Paul and Evans were the first to note that all these processes are governed by the same Arrhenius law [30].

Multiple researchers have proposed wear models that relate wear rate to temperature in an Arrhenius-style equation. Takeyama–Murata's model related wear divided by time, dW/dt , as a function of temperature [29]

$$\frac{dW}{dt} = A \exp\left(\frac{-E_a}{RT}\right) + \text{abrasive term} \quad (1)$$

Here, A is a pre-exponential constant, E_a is the activation energy, R is the universal gas constant, and T is temperature in degrees Kelvin. Their abrasive term was a function of feed rate and sliding speed. Usui et al. re-derived the model of Trigger and Chao, which similarly says dW/dt is an exponential function of temperature [28,31]. However, this model also states that the wear rate is proportional to contact normal stress and sliding speed:

$$\frac{dW}{dt} = A \sigma_n v_s \exp\left(\frac{-B}{T}\right) \quad (2)$$

Here, A is a pre-exponential constant, σ_n is normal contact stress, and v_s is sliding speed. B represents combined temperature-dependent effects of thermal softening and diffusion of wear asperities into the workpiece and probability that a wear particle will occur. However, this is functionally the same as the E_a/R in Takeyama's model. Jiang et al. defined wear rate as the Archard wear coefficient in units of volume, W , divided by sliding distance, s , divided by contact force, F , in their study of diamond-like coatings rubbing on steel substrates [32,33]. They stated that this wear rate follows the following form:

$$K = \frac{W}{sF} = K_0 \frac{1}{v_s} \exp\left(\frac{-E_a}{RT}\right) \quad (3)$$

If force is considered invariant with sliding speed in Eq. (3) and abrasive terms are neglected in Eq. (1), then Takeyama's and Jiang's

¹ Certain commercial equipment, instruments, or materials are identified in this paper to foster understanding. Such identification does not imply recommendation or endorsement by the National Institute of Standards and Technology, nor does it imply that the materials or equipment identified are necessarily the best available for the purpose.

models are the same. If both sides of Takeyama's model in Eq. (1) are divided by v_s , the left term becomes wear divided by distance, dW/ds , like Jiang's model in Eq. (3). These simplifications are valid since tool forces in diamond turning have been shown to be largely independent of cutting speed [34]. Also, abrasive effects of low carbon steel were shown to be negligible on diamond tools since other workpiece materials of similar hardness but non-reactive chemistry result in comparable wear at thousand times further cutting distance [13]. If both sides of Eq. (2) are divided by v_s to put the wear rate into dW/ds form, Ueda's model loses the proportionality relationship to $1/v_s$ given in Takeyama's and Jiang's models. In this paper, an Arrhenius-type model representative of Takeyama's and Jiang's is used and simplified to either of the interchangeable forms describing wear/time or wear/distance:

$$\frac{dW}{dt} = A \exp\left(\frac{-E_a}{RT}\right) \Leftrightarrow \frac{dW}{ds} = \frac{A}{v_s} \exp\left(\frac{-E_a}{RT}\right) \quad (4)$$

One point of interest is that Takeyama and Jiang arrived at the same wear rate function, but through analyzing entirely different physical mechanisms. Takeyama et al. based their model on the theory of diffusion and Fick's law. Jiang and Arnell based their model on a chemically activated crack propagation model that gave the generation of wear debris particles as a function of temperature. Paul et al. reviewed multiple other possible physical and chemical mechanisms that allow carbon to be removed from a diamond tool, including diffusion, catalytic reaction, and formation of a number intermediary reaction complexes. They also noted that most of these mechanisms they and others describe follow an Arrhenius-type law, but it would be difficult to experimentally distinguish which contribute most to wear [30]. For this reason, individual contributing factors are not discussed in this paper, but it is shown that single values of A and E_a can describe wear rates over a wide range of cutting speeds. An approach similar to the one used by Jiang is presented here, which involves the following steps:

- (1) Obtain a best-fit functional relationship between tool temperature, cutting speed, and depth of cut. Jiang used the friction-heating model of Archard [35]. This paper presents temperature determined through finite element simulations.
- (2) Perform diamond turning experiments over a wide range of cutting speeds and measure tool wear rate via EBID method.
- (3) Evaluate the empirical constants, E_a and A , in the Arrhenius wear model by relating measured wear and modeled tool temperatures.

Similar to Jiang, results are plotted as dW/ds as a function of cutting speed. Wear rates determined experimentally are compared

against the model. The model is used to explain the experimental results from this paper and compared to similar observations made by others researching thermo-chemical diamond wear.

3. Finite element models for tool temperature

As previously mentioned, tool temperatures are determined using finite element modeling via the commercial FEM code. Since the contact width in diamond turning is typically two orders of magnitude or greater than the depth of cut, the process is essentially two-dimensional. This assumes zero strain and zero heat transfer along the out-of-plane direction. Two-dimensional cutting simulations are therefore used in the FEM software. Relationships between peak temperature rise (ΔT), cutting speed (v_s), and depth of cut (d_c) are obtained by using Matlab's surface fit tool (sftool) to determine what function best describes this relationship.

3.1. Simulation setup

A total of 32 simulations were created varying the depth of cut and cutting speed. Depth of cut values were 0.5 μm , 0.75 μm , 1 μm , and 2 μm . Cutting speed values were 0.01 m/s, 0.05 m/s, 0.1 m/s, 0.5 m/s, 1 m/s, 2 m/s, 3 m/s, and 4 m/s. The 2D tool model was 100 μm tall by 80 μm wide with a 0° rake angle, 6° clearance angle, and 200 nm edge radius. The workpiece model was 150 μm in length and 50 μm tall. The back and top of the tool and bottom of the workpiece had isothermal boundary conditions at the ambient temperature of 20 °C, shown in Fig. 1. All other surfaces in the FEM model had adiabatic boundary conditions. The isothermal boundaries remove heat from the tool model, and proximity of these boundaries to the heat source will create erroneously low temperature values and rapid transient heating and cooling. Others conducting FEM or analytical modeling of diamond tool temperature utilize semi-infinite boundaries, which are likely a better model assumption since the actual diamond is several millimeters in scale [17,24]. However, infinite boundary elements are not available in the FEM software used, therefore the tool model is made sufficiently large such that doubling tool model area resulted in less than 1 °C increase in peak tool temperature.

Workpiece and tool third-dimensional depth was 1 mm, though this does not affect any temperature values as heat transfer along the third-dimension is neglected in the model. American Iron and Steel Institute (AISI) 1215 steel was not available in the software material library. AISI 1118 steel has similar mechanical and thermal

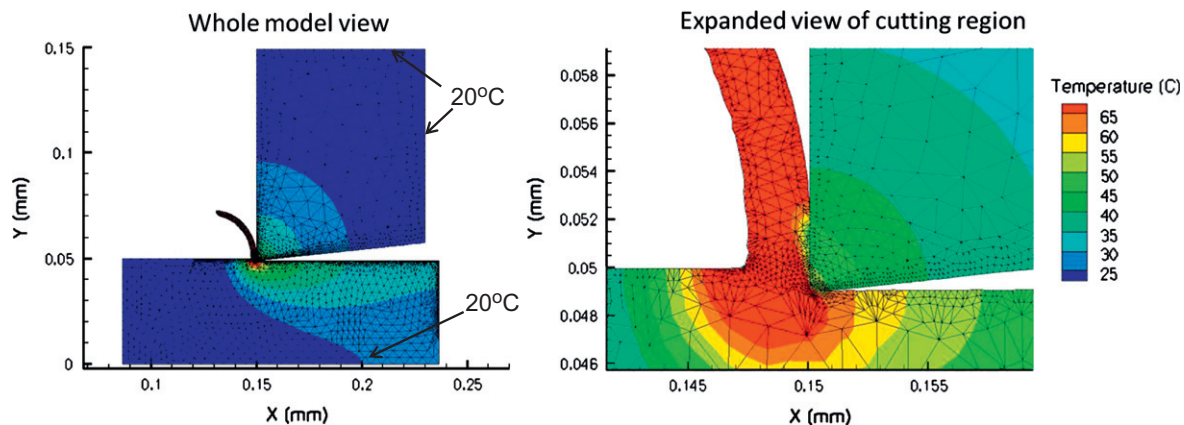


Fig. 1. Model geometry and mesh for AdvantEdge cutting simulations. Example temperature contours are for the 1 μm depth of cut, 3 m/s simulation results.

properties as 1215, and was chosen as the workpiece material. Tool wear was single crystal diamond.

Tool wear occurs simultaneously with cutting, which inevitably alters the chip formation and heat transfer characteristics. Worn tool shapes were not incorporated into the FEM cutting simulations. It is shown later that the depth of wear may be on the same order as the depth of cut. While this likely has an effect on the location of the hottest point on the worn tool edge and the magnitude of the peak temperature, this is not taken into account with these FEM simulations. However, it is later shown that the Arrhenius-type wear model applies regardless of large variation in worn tool edge shapes. Further analysis with worn tool shapes may provide better understanding of how these shapes progress and how temperature varies along the changing contact region.

3.2. Cutting simulation results

Maximum tool temperatures occurred on the cutting edge radius of the tool model. These values were extracted from the FEM simulations and steady state temperature values were obtained by taking the average temperature value in the range where the tool was no longer heating and had not yet reached the edge of the workpiece. Steady state temperature rise, cutting speed, and depth of cut values were supplied to the surface fitting tool. Based on the observed trend in resulting temperatures, a linear relationship with speed and power-function relationship with depth of cut was surmised. A custom fit equation based on this observation was supplied to the surface fit tool with results shown in Fig. 2. The custom equation showed a linear rise in temperature with cutting speed of $11.81\text{ }^\circ\text{C s m}^{-1}$ at a depth of cut of $1\text{ }\mu\text{m}$. This results in the form given in Eq. (5), with depth of cut d_c normalized by $1\text{ }\mu\text{m}$ to make the base unit-less ($\mu\text{m}/\mu\text{m}$), and T_0 ambient temperature of $20\text{ }^\circ\text{C}$:

$$\Delta T = T - T_0 = kv_s d_c^n \quad (5)$$

Trigger and Chao also saw a linear relationship with cutting speed in non-ultraprecision turning of steel with carbide tools [36]. Ueda et al. also measured a highly linear relationship between tool temperature rise and cutting speed in their two-color pyrometer measurements [16]. Based on Ueda's reported values, a temperature rise approximately $6.5\text{ }^\circ\text{C s m}^{-1}$ resulted on copper and aluminum workpieces with cutting speed range of 6.7 m/s to 15 m/s . They used a constant depth of cut of $10\text{ }\mu\text{m}$ for all experiments, so the effects of this parameter cannot be compared. Though Ueda's speeds exceed those utilized in this paper, Trigger and Chao's linear relationship between temperature and speed was observed down to 0.56 m/s (110 ft/min).

Using this semi-empirical temperature relationship, the thermo-chemical wear model is formed. Temperature as a function of cutting speed and depth of cut given by Eq. 5 is substituted into Eq. (4) to give dW/ds as a function of cutting speed and empirical constants

$$\frac{dW}{ds} = \frac{A}{v_s} \exp\left(\frac{-E_a}{R(kv_s d_c^n + T_0)}\right) \quad (6)$$

The constants k and n are determined through FE modeling, which leaves A and E_a determined empirically from wear experiments. Once determined, dW/ds becomes solely a function of cutting speed v_s with several interesting properties. For low v_s , the rate dW/ds is proportional to $1/v_s$, meaning the wear per unit distance decreases with speed. As v_s increases, thus increasing temperature linearly, the exponent in Eq. (6) contributes more causing dW/ds to reach a minimum and start increasing with v_s . The minimum is determined by taking the derivative of dW/ds with respect to v_s and setting equal to zero. This calculation is left to the reader.

4. Machining experiments and tool wear measurement

Given the relationship between cutting speed and temperature, a relationship between cutting speed and measured wear values is necessary to complete the Arrhenius model. When diamond turning with a round tool with feed direction parallel to the cutting edge, recession of the edge due to wear will reduce the true depth of cut by the recess distance. This will inevitably change the cutting conditions with time and complicate any relationship of temperature to wear. Also, the resulting wear may not be continuous along the cutting edge, which makes quantifying wear difficult. To maintain a constant depth of cut regardless of wear, a machining setup is created that continuously feeds the tool into the workpiece in a direction perpendicular to the cutting edge in the depth of cut direction. Orthogonal cutting geometry is also used in all machining experiments with a workpiece width narrower than the tool edge. This minimizes variation in cutting conditions along the cutting edge. While this geometry is not directly analogous to a facing operation, it is more applicable to modeling of the thermo-chemical wear process by reducing the number of variables.

4.1. Machining setup

The same single crystal diamond tool was used in all experiments, with re-sharpening performed by the tool supplier between

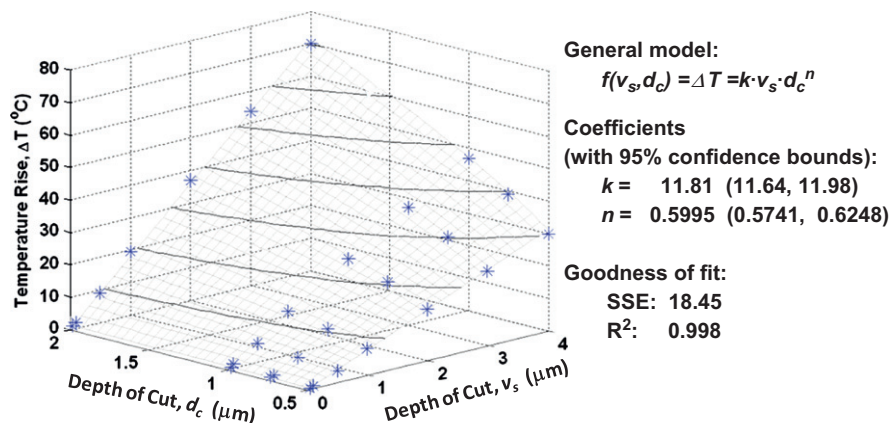


Fig. 2. Results from Matlab surface fit tool (sftool) relating temperature rise to cutting speed and depth of cut obtained from FE models. Goodness of fit statistics include summed square of residuals (SSE) and coefficient of determination (R -squared).

each cutting speed experiment set. Edge radius was below 50 nm after sharpening and confirmed in SEM measurements. This tool was a 2.28 mm wide, straight-edged tool with rake face nominally aligned with the (001) crystallographic plane and chip flow occurring along the $\langle 100 \rangle$ direction. This should be noted since crystallographic direction can have a large impact on wear rate of diamond and diamond tools [37–38]. Machine setup used a rake face of 0° and clearance angle of 6° . To complete machining at workpiece velocities ranging from 0.001 m/s to 4 m/s, several machining setups had to be made. Fig. 3 shows the three ranges of cutting speed geometry used in cutting. All workpieces were AISI 1215 steel machined from the same stock. In the low speed experiments (2 mm/s to 8 mm/s), cutting speed is set directly by the diamond turning machine (DTM) axes. Mid and high speed machining tests controlled the cutting speed by varying the radius to the cut surface and spindle speed. Mid and high speed tests were conducted on an ASG 9000 diamond turning machine, and low speed tests were conducted on a Nanoform 600. The Nanoform had an available workpiece mounting post where the ASG would have required fabricating a holder and mounting to the spindle. An oil-based streamer cutting fluid was used in all cutting tests.

Initially, high speed cutting tests were conducted with workpiece width of 1 mm. This required wear measurements to be taken after each cut. Later, slow and mid speed experiments utilized narrower workpieces (later referred as “fin”), shown in Fig. 4. Workpiece width of 0.25 mm enabled three distinct wear zones on the 2.28 mm wide tool. A fourth zone was used to remove the top oxidized layer of the fin and remove runout so that cutting initiated in a continuous manner. For the high speed experiments, runout and oxide layer were removed with a carbide tool.

4.2. Wear measurement

After machining, diamond tool wear was measured in a field emission SEM via electron beam induced deposition (EBID) [11–13]. This process is summarized in Fig. 5. A stripe of hydrocarbon contamination is formed along the cutting edge of a worn diamond tool by scanning a focused electron beam along the diamond surface. This stripe provides contrast to allow the cutting edge to be determined from the SEM image. SEM images are then stretched vertically according to $1/\cos(\theta)$ where θ is the tilt angle of the tool toward the viewing plane (nominally 45°). A Matlab code allows the user to select pixels from the SEM image that traces the EBID stripe or worn tool cross-section. The calculated angle between the rake and clearance face of the stretched SEM image is compared against the included angle of the actual tool (90° minus clearance angle or 84° for the tool used in this paper). The vertical image size is then readjusted until the image included angle is within $\pm 1^\circ$ of the real tool included angle. This readjustment changes the vertical image size $< 5\%$ from the $1/\cos(\theta)$ calculation under normal circumstances, but

provides more accurate scaling based on the true tool geometry rather than the SEM goniometer stage angle. The Matlab code then changes the scale of the image from pixels to microns according to the SEM image measure bar, and rotates the cross-section to align with other collected cross-sections for direct comparison. Worn cross-section area is determined by calculating the area enclosed by the EBID stripe and two best-fit lines that run along the EBID stripe where it contacts unworn clearance and rake faces. Worn tool cross-sections made from EBID images are rotated and aligned so that the original tool point exists at the origin of the plot. Lines corresponding to the rake face of the tool align with the y-axis of the plots.

The general shape of the wear varied between the multi-speed experiment sets as well, shown in Figs. 6–9. The cutting direction, indicated in Fig. 6, is the same for each figure. High speed experiments shown in Fig. 6 yielded a short wear land that formed at a consistent angle to the cutting direction [13]. Low speed tool shapes in Fig. 8 yielded large, flat wear lands that were nominally parallel to the cutting direction and perpendicular to the rake face. These resemble the wear pattern observed after DT of 6061 aluminum, though the scale of the wear is much larger from steel [13]. A flat wear land region was observable on the lowest of the mid speed tool profiles (71 mm/s cutting speed) in Fig. 7 which resemble those of the low speed experiment set. The highest speed of the mid speed profiles (284 mm/s) were more rounded and resembled the shape of the high speed experiment set. This indicates a transition between low and high speed wear forms. Low speed tools also showed grooving along the cutting direction on the clearance side of the tool observed by Brinksmeier et al. [8], though this is not visible in Fig. 8.

Uncertainty of EBID worn area measurements stems from two main contributors 1) resolution of the edge between the EBID stripe and diamond surface and 2) pixel selection in the Matlab code. Intrinsic resolution of the SEM used is not a factor. The SEM is calibrated bi-monthly with a NIST traceable reference standard resulting in a spatial resolution of 6.2 nm at the 4 kV accelerating voltage used for the EBID process. EBID stripe growth rate

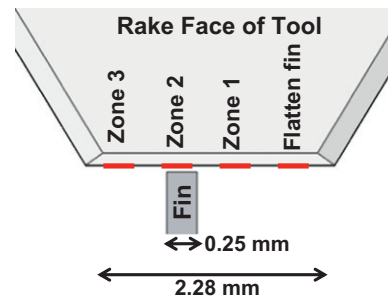


Fig. 4. Cutting zones on straight-edged diamond tool used in low and mid speed orthogonal cutting experiments.

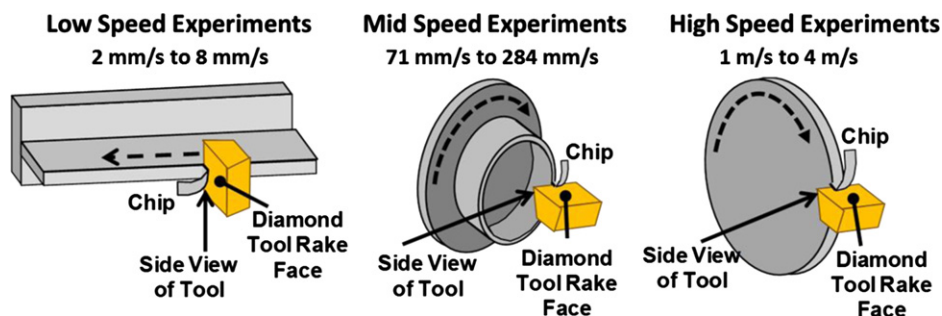


Fig. 3. Multi-speed machining experiment setup for three speed ranges.

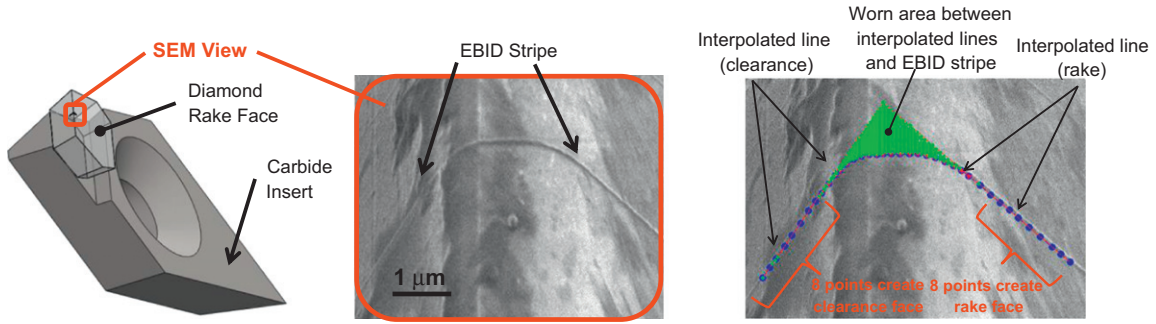


Fig. 5. Left: viewing angle of EBID stripe on the diamond edge. Center: example EBID image. Right: worn area and cross-section measurement via Matlab code.

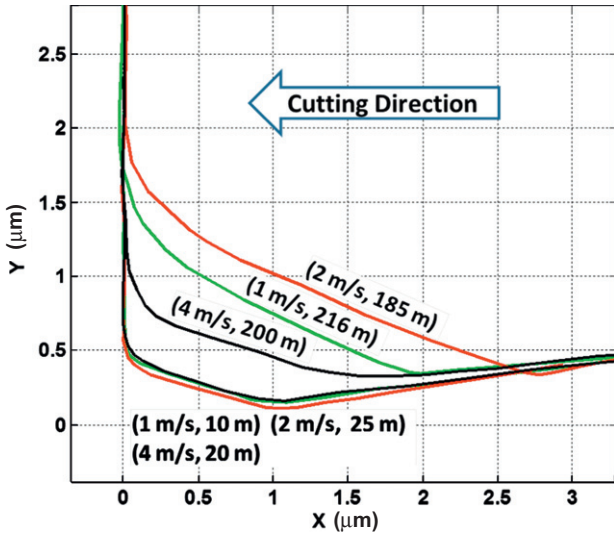


Fig. 6. Worn tool cross-sections for high speed cutting experiments.

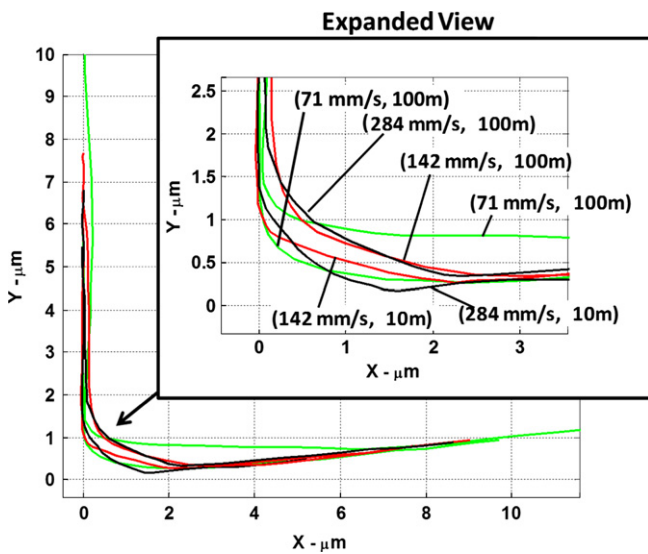


Fig. 7. Worn tool cross-sections for mid speed cutting experiments.

depends on the unknown contaminant conditions in the SEM chamber, so user experience and ‘trial-and-error’ procedure are necessary to create a measurable stripe. It was not possible to make enough EBID lines to calculate statistically an uncertainty value for each wear area measurement. Based on repeated

measurements of a single image, the authors estimate the Type B expanded uncertainty of the 2D worn area is 15% ($k=2$).

The 2D cross-sectional shapes appear to transition from a flat wear land formed perpendicular to the cutting direction for low speeds to an upturned wear land that formed at an angle to the cutting direction at high speeds. The mid speed experiments appeared as a transition from the low to high speed forms. The scale of wear divided by machining distance also varied dramatically between the three experiment sets. Two example comparisons are made in Fig. 9 that show how tool wear at low speeds and short distance yielded higher wear than mid speed and long distance. Also, mid speed at short distance yielded more wear than high speed at short distance. This demonstrates a trend of decreasing dW/ds as speed increases.

Two-dimensional wear areas were calculated using the Matlab EBID image analysis code with results shown in Fig. 10. Observation of tools in the SEM showed a constant level of wear along the width of the wear region along the cutting edge. The wear divided by cut distance dW/ds changed from a low rate to higher rate for low speed experiments, and from high rate to low rate for the mid and high speed experiments.

5. Arrhenius wear model results

Finite element models used to determine the temperature expression in Fig. 2 did not include cutting speeds in the range of the low speed experiments. Assuming the formula determined in Fig. 2 and depth of cut of 1 μm, temperature of the low speed experiments would only vary between 0.02 °C and 0.1 °C above ambient temperature of 20 °C. These points would all lie at the same x -axis location on an Arrhenius plot and not provide for determining the Arrhenius coefficients. For this reason, low speed wear data is not used in the formulation of Arrhenius empirical constants. Low speed data is still included in the comparison of results.

For each speed shown in Fig. 10, the wear area divided by distance rates is not constant. Wear rates between zero cut distance and the first cut distance create a first rate value or slope. Rates between the first and second cut distance create a second slope. This creates 18 slope values in all. The dW/ds rates were converted to dW/dt by dividing by the respective workpiece velocities. Again, low speed data is ignored for formulation of Arrhenius coefficients, which leaves 12 slope values shown in the Arrhenius plot in Fig. 11. Temperatures are determined using finite element data from Fig. 2 and Eq. (5) using the 1 μm depth of cut. Three best-fit linear functions are created using the T^{-1} axis. These three functions utilize data from the first dW/ds slope values from Fig. 10, the second slope values, and all 12 values. Corresponding Arrhenius coefficients are given at right.

Given k and n determined from FE temperature modeling, and E_a and A determined from either of the fit lines in Fig. 11, Eq. (6)

becomes dW/ds as a smooth function of v_s . The resulting model curves are plotted against the eighteen dW/ds wear rate points from the three experiment sets in Fig. 10. Though low speed data was not used to determine Arrhenius coefficients, it is presented for comparison.

Fig. 12 shows how the Arrhenius-type wear model trends when coupled with a linear relationship between cutting speed and temperature. The model and resulting curve explain how dW/ds decreases as speed increases, as observed by the comparative wear measurements in Fig. 9. The wear minimum is calculated by taking the derivative of dW/ds with respect to v_s in Eq. (6), setting equal to zero, and solving for v_s . This results in $v_s^{\min} = 2.7$ m/s for the line corresponding to $E_a = 27.1$ kJ/mol in Fig. 12.

6. Discussion

Previous studies present results that are related to those described this paper. The process of thermal modeling, wear measurement, and relationship to an Arrhenius-type model used here is directly analogous to the result of Jiang et al. [33]. Though their study was for diamond-like carbon films sliding on tungsten carbide, they arrived at similar conclusions: (1) a linear relationship with sliding speed and temperature, (2) minimum value of dW/ds at a specific sliding speed (theirs was 0.25 m/s), and (3) relatively low activation energy near 27 kJ/kmol. This activation energy was well below those reviewed as potential tool wear reaction mechanisms by Paul and Evans et al. [30], or results from static diffusion tests [39]. This is likely due to the fact that a new clean surface of workpiece material was under constant contact with the tool. While static diffusion specimens eventually saturate with diffused material, a concentration gradient is unable to form in the moving chip, thus maintaining a higher rate of diffusion. This idea was discussed by Molinari and Nouari, who added an advection term to the classic 1D diffusion equation to analyze wear of carbide tools [40]. However, they didn't compare static to advection-diffusion models, and how this would relate to empirically determined activation energy. The effect of advection on the empirically determined activation energy also obscures the ability to differentiate the multiple potential chemical reaction mechanisms outlined by Paul and Evans et al. The contribution of individual mechanisms, as they pertain to workpiece alloy composition, cannot be determined without expanding the number of alloys tested. It should be noted that the empirical constants determined in this paper are specific to the steel alloy and diamond type used.

Other studies of chemical diamond tool wear provide similar experimental results, though not in the context of a thermochemical wear model. Brinksmeier and Glabe diamond turned Ck45N (AISI 1045) steel and measured wear via atomic force microscope [8]. They also saw variation in the tool wear shape with cutting speed and a minimum level of wear that occurred at

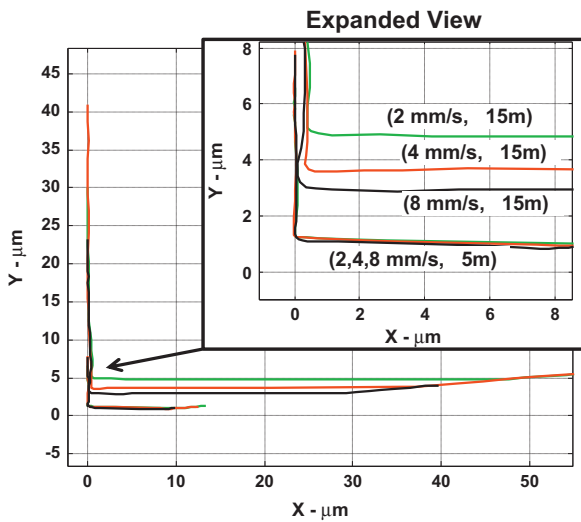


Fig. 8. Worn tool cross-sections for low speed cutting experiments.

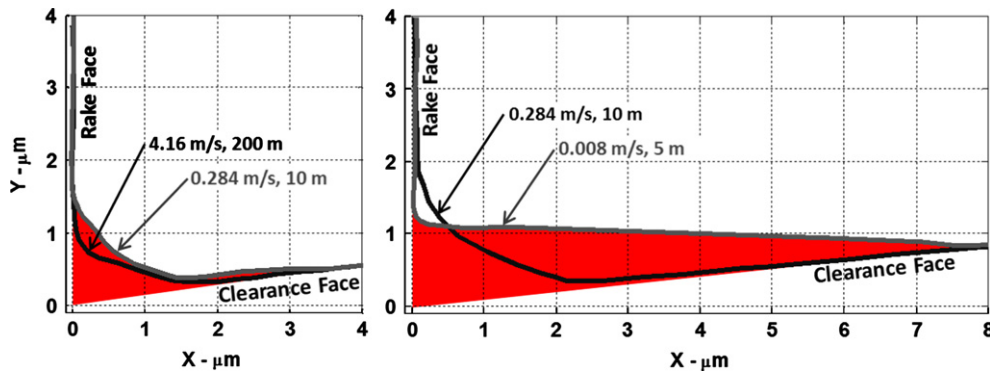


Fig. 9. EBID cross sections of worn tool edges cutting AISI1215 steel comparing different levels of wear for different workpiece velocities. Left: mid speed and low distance vs. high speed at long distance. Right: low speed at low distance vs. mid speed at long distance.

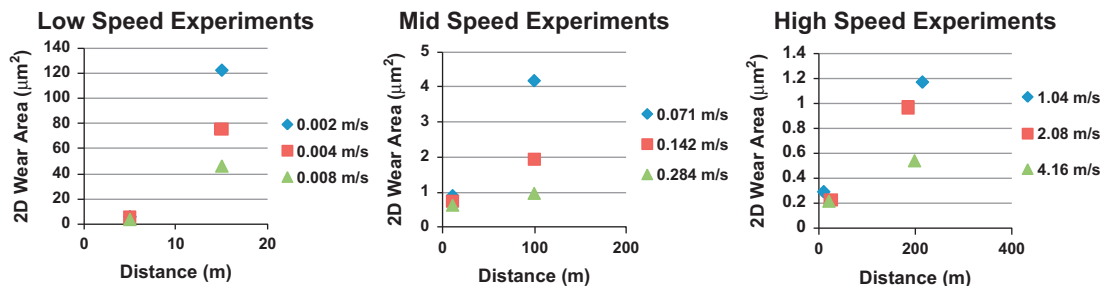


Fig. 10. 2D wear areas for the low, mid, and high speed cutting experiments on AISI1215 steel

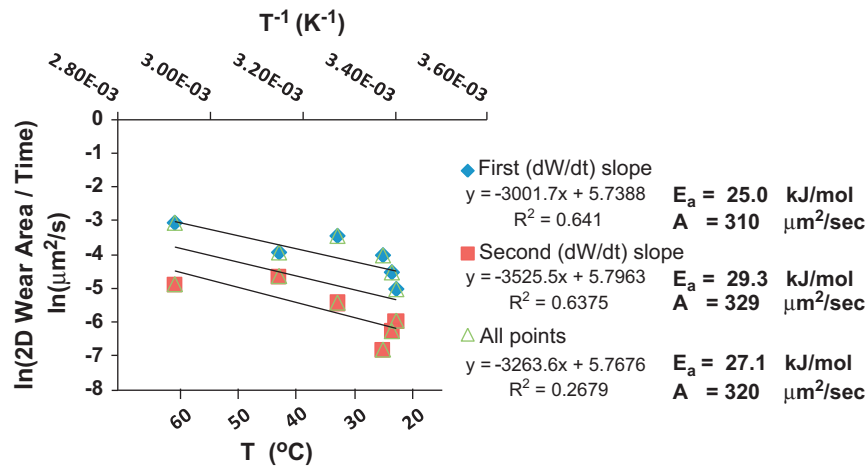


Fig. 11. Arrhenius plot of mid and high speed 2D wear area change vs. inverse of tool temperature determined from finite element models.

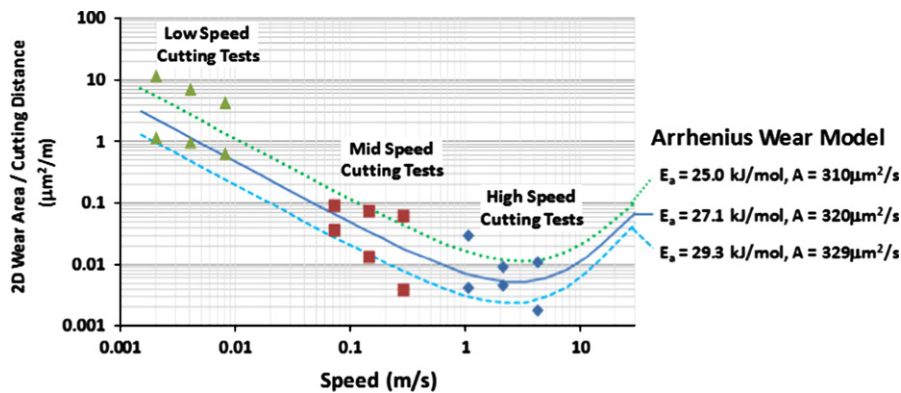


Fig. 12. Arrhenius wear model and experimentally determined wear rates over four orders of magnitude of cutting speed.

approximately 1.2 m/s cutting speed. Brinksmeier verified that there is a minimum similar to the one in Fig. 12, though high speed experiments were not performed in this paper and the value of the minimum was not determined experimentally. Thornton and Wilks observed that the wear rate (defined as worn surface area of the tool divided by formed surface area of the part in units of $10^{-7} \text{ mm}^2/\text{mm}^2$) decreased as surface speed increased from 0.2 m/s to 11 m/s [41,42]. They also noted that wear rate increased dramatically when they attempted to machine at very high speed (30 m/s). Thornton and Wilks, and later Paul and Evans et al., surmised that high levels of wear at low speeds were due to oxygen infiltrating the cutting zone and assisting the reaction between workpiece and tool materials. Similarly, wear was reduced at higher speeds since there was not enough time for oxygen to enter the cutting zone. Though availability or lack of oxygen may indeed play a role in diamond wear, the Arrhenius type wear model proposed here accounts for these wear rates without assuming multiple reaction mechanisms.

Another important point is that Usui's wear model does not represent the experimental data shown in Figs. 10 and 12. If constant stress value is assumed, Usui's model would predict dW/ds to increase as cutting speed increases over the range of speeds used in this paper. At higher speeds, however, Usui's wear model may well represent the right-side of the wear minimum in Fig. 12. Regardless, the functional form of Usui's model does not predict a minimum.

Ultimately, the purpose of diamond turning is to produce excellent quality surface finish, and the purpose of understanding

tool wear is to maximize the amount of surface machined before replacement of a tool. This study does not address the complicated nature between tool wear and surface finish generation. In addition, direct diamond turning of ferrous alloys by conventional methods is not economically feasible, even if machining at the minimum of Fig. 12. However, this baseline understanding of the process mechanics may provide for optimization of other processes that utilize diamond to cut ferrous alloys. Tailoring of sliding speed to achieve the wear minimum shown in Fig. 12 has the potential to optimize proven methods such as grinding or vibration-assisted machining.

The Arrhenius plot in Fig. 11 does not include the low speed experiments. Given the temperature vs. speed relationship in Fig. 2, these speeds would produce temperatures very near ambient, and occur near the $3.42 \times 10^{-3} \text{ K}^{-1}$ point on the x-axis. These would contribute little to the slope and intercept linear best-fit calculation used to determine activation energy and pre-exponential constant. High speed, higher temperature data better evaluates these factors.

7. Conclusions

- (1) A thermo-chemical wear model for diamond tool wear on ferrous alloy was proposed based on an Arrhenius-type relationship between wear and temperature. Finite element modeling provided tool temperature values, while diamond

turning experiments provided wear results. The model explains how low speed machining of steel results in higher levels of wear over the same cutting distance than high speed machining. It also shows a minimum dW/ds occurs near 2.0 m/s cutting speed for the AISI 1215 material tested.

- (2) Activation energy, E_a , was found to lie between 25 kJ/mol and 29.3 kJ/mol. This is much lower than estimated values by other researchers.
- (3) Geometric form of the 2D worn tool cross-section varied over each order of magnitude of speed. Low speed machining (2–8 mm/s) resulted in worn tools with large wear land parallel to the cutting direction. High speed machining (1–4 m/s) resulted in short wear lands that formed at an angle to the cutting direction. Mid speed experiments (71–284 mm/s) showed a transition between the low and high speed forms.

Acknowledgments

The experimental research reported in this paper was conducted at North Carolina State University while the primary author was affiliated with the university. Primary funding for this work was by National Science Foundation Grant CMMI-0800560 monitored by G. Hazelrigg. Third Wave systems provided academic licensing and technical support for AdvantEdge software. Chardon Tools supplied the diamond tools and tool sharpening used in the machining experiments.

References

- [1] N. Ikawa, T. Tanaka, Thermal aspects of wear of diamond grain in grinding, *CIRP Annals Manufacturing Technology* 19 (1971) 153–157.
- [2] D. Crompton, W. Hirst, M.G.W. Howse, The wear of diamond, *Proceedings of the Royal Society of London A* 333 (1973) 435–454.
- [3] C.J. Evans, J.B. Bryan, Cryogenic diamond turning of stainless steel, *CIRP Annals Manufacturing Technology* 40 (1991) 571–575.
- [4] J.M. Casstevens, Diamond turning of steel in carbon-saturated atmospheres, *Precision Engineering* 5 (1983) 9–15.
- [5] T. Moriwaki, E. Shamoto, Ultraprecision diamond turning of stainless steel by applying ultrasonic vibration, *CIRP Annals Manufacturing Technology* 40 (1991) 559–562.
- [6] S. Asai, Y. Taguchi, K. Horio, T. Kasai, A. Kobayashi, Measuring the very small cutting-edge radius for a diamond tool using a new kind of SEM having two detectors, *CIRP Annals Manufacturing Technology* 39 (1990) 85–88.
- [7] D.A. Lucca, Y.W. Seo, R. Komanduri, Effect of tool edge geometry on energy dissipation in ultraprecision machining, *CIRP Annals Manufacturing Technology* 42 (1993) 83–86.
- [8] E. Brinksmeier, R. Gläbe, Advances in precision machining of steel, *CIRP Annals Manufacturing Technology* 50 (2001) 385–388.
- [9] W. Gao, T. Motoki, S. Kiyono, Nanometer edge profile measurement of diamond cutting tools by atomic force microscope with optical alignment sensor, *Precision Engineering* 30 (2006) 396–405.
- [10] X.P. Li, M. Rahman, K. Liu, K.S. Neo, C.C. Chan, Nano-precision measurement of diamond tool edge radius for wafer fabrication, *Journal of Materials Processing Technology* 140 (2003) 358–362.
- [11] J.D. Drescher, Scanning electron microscopic technique for imaging a diamond tool edge, *Precision Engineering* 15 (1993) 112–114.
- [12] M. Shi, B. Lane, C.B. Mooney, T.A. Dow, R.O. Scattergood, Diamond tool wear measurement by electron-beam-induced deposition, *Precision Engineering* 34 (2010) 718–721.
- [13] B.M. Lane, M. Shi, T.A. Dow, R.O. Scattergood, Diamond tool wear when machining Al6061 and 1215 steel, *Wear* 268 (2010) 1434–1441.
- [14] E. Whittenton, R. Ivester, H.W. Yoon, Simultaneous visible and thermal imaging of metals during machining, *Proceedings of SPIE* 5782 (2005) 71–82.
- [15] H. Yoshioka, H. Hashizume, H. Shinn, In-process microsensor for ultraprecision machining, *IEEE Proceedings—Science, Measurement and Technology* 151 (2004) 121–125.
- [16] T. Ueda, M. Sato, K. Nakayama, The temperature of a single crystal diamond tool in turning, *CIRP Annals Manufacturing Technology* 47 (1998) 41–44.
- [17] R. Komanduri, Z.B. Hou, Thermal modeling of the metal cutting process: Part I—temperature rise distribution due to shear plane heat source, *International Journal of Mechanical Sciences* 42 (2000) 1715–1752.
- [18] R. Komanduri, Z.B. Hou, Thermal modeling of the metal cutting process—Part II: temperature rise distribution due to frictional heat source at the tool–chip interface, *International Journal of Mechanical Sciences* 43 (2001) 57–88.
- [19] R. Komanduri, Z.B. Hou, Thermal modeling of the metal cutting process—Part III: temperature rise distribution due to the combined effects of shear plane heat source and the tool–chip interface frictional heat source, *International Journal of Mechanical Sciences* 43 (2001) 89–107.
- [20] N.A. Abukhshim, P.T. Mativenga, M.A. Sheikh, Heat generation and temperature prediction in metal cutting: A review and implications for high speed machining, *International Journal of Machine Tools and Manufacture* 46 (2006) 782–800.
- [21] J.T. Carroll III, J.S. Strenkowski, Finite element models of orthogonal cutting with application to single point diamond turning, *International Journal of Mechanical Sciences* 30 (1988) 899–920.
- [22] W.J. Zong, T. Sun, D. Li, K. Cheng, Design criterion for crystal orientation of diamond cutting tool, *Diamond and Related Materials* 18 (2009) 642–650.
- [23] W.J. Zong, D. Li, K. Cheng, T. Sun, Y.C. Liang, Finite element optimization of diamond tool geometry and cutting-process parameters based on surface residual stresses, *International Journal of Advanced Manufacturing Technology* 32 (2007) 666–674.
- [24] T. Moriwaki, N. Sugimura, S. Luan, Combined stress, material flow and heat analysis of orthogonal micromachining of copper, *CIRP Annals Manufacturing Technology* 42 (1993) 75–78.
- [25] H.Y. Wu, W.B. Lee, C.F. Cheung, S. To, Y.P. Chen, Computer simulation of single-point diamond turning using finite element method, *Journal of Materials Processing Technology* 167 (2005) 549–554.
- [26] K. Woon, M. Rahman, F. Fang, K. Neo, K. Liu, Investigations of tool edge radius effect in micromachining: a FEM simulation approach, *Journal of Materials Processing Technology* 195 (2008) 204–211.
- [27] R. Komanduri, M. Shaw, On the diffusion wear of diamond in grinding pure iron, *Philosophical Magazine* 34 (1976) 195–204.
- [28] K. Trigger, B. Chao, The mechanism of crater wear of cemented carbide tools, *Transactions of ASME* 78 (1956) 1119–1126.
- [29] H. Takeyama, R. Murata, Basic investigation of tool wear, *Transactions on ASME Journal Engineering for Industry* 85 (1963) 33–38.
- [30] E. Paul, C.J. Evans, A. Mangamelli, M.L. McGlaufflin, R.S. Polvani, Chemical aspects of tool wear in single point diamond turning, *Precision Engineering* 18 (1996) 4–19.
- [31] E. Usui, T. Shirakashi, T. Kitagawa, Analytical prediction of cutting tool wear, *Wear* 100 (1984) 129–151.
- [32] J.F. Archard, W. Hirst, The wear of metals under unlubricated conditions, *Proceedings of the Royal Society of London A* 236 (1956) 397–410.
- [33] J. Jiang, R.D. Arnell, The effect of sliding speed on wear of diamond-like carbon coatings, *Wear* 218 (1998) 223–231.
- [34] C. Arcona, T.A. Dow, An empirical tool force model for precision machining, *Journal of Manufacturing Science and Engineering* 120 (1998) 700–707.
- [35] J.F. Archard, The temperature of rubbing surfaces, *Wear* 2 (1959) 438–455.
- [36] K. Trigger, B. Chao, Temperature distribution at the tool–chip interface in metal cutting, *Transactions of ASME* 77 (1955) 1107–1120.
- [37] Z.J. Yuan, J.C. He, Y.X. Yao, The optimum crystal plane of natural diamond tool for precision machining, *Annals-Manufacturing Technology* 41 (1992) 605–608.
- [38] E.M. Wilks, J. Wilks, The resistance of diamond to abrasion, *Journal of Physics D* 5 (1972) 1902.
- [39] S. Shimada, H. Tanaka, M. Higuchi, T. Yamaguchi, S. Honda, K. Obata, Thermochemical wear mechanism of diamond tool in machining of ferrous metals, *CIRP Annals Manufacturing Technology* 53 (2004) 57–60.
- [40] A. Molinari, M. Nouari, Modeling of tool wear by diffusion in metal cutting, *Wear* 252 (2002) 135–149.
- [41] A.G. Thornton, J. Wilks, Tool wear and solid state reactions during machining, *Wear* 53 (1979) 165–187.
- [42] A.G. Thornton, J. Wilks, The wear of diamond tools turning mild steel, *Wear* 65 (1980) 67–74.